Supporting Information

Pearce et al. 10.1073/pnas.1710339114

SI Text

Calculating WLP Surface Area on Early Earth

The earliest fairly conclusive evidences of life are in the form of light carbon signatures in graphite globules formed from marine sediments, and stromatolite fossils, both which are dated to be 3.7 Gy old (4, 5). Therefore, nucleobase deposition in WLPs and subsequent reactions to form nucleotides and RNA would have occurred sometime between ∼4.5 and 3.7 Ga.

Once Theia impacted the proto-Earth ∼50 My after Solar System formation, it may have only taken 10 My to 100 My for the magma mantle to cool (30). Furthermore, basic evidence (from the zircon oxygen isotope record) exists of crustal material interacting with liquid water at or near Earth's surface since 4.3 Ga (48). Such evidence makes it clear that Earth had a hydrosphere at that point, and therefore could have formed WLPs on any rising continental crust.

An estimate of the surface area of WLPs on early Earth has not been previously attempted; however, it is often suggested that they were typical on early Earth continents (33, 44, 48). Water-deposited sediments dated at 3.8 Ga indicate early erosion and transport of sediment; therefore, at that time, at least some continental mass must have been exposed above sea level, on which WLPs could have formed (33).

Continental Crust Growth Model. The number of WLPs present at any given time depends on the fraction of continental crust above sea level. Calculations from a continental crust growth model show a linear formation of early crust, increasing from 0 to 12.8% of today's crustal surface area from 4.5 Ga to 3.7 Ga (29). This is expressed in the following equation:

$$f_{cr} = 0.16t, \qquad \textbf{[S1]}$$

where f_{cr} is the fraction of today's crustal surface area, and t is the time in gigayears ($t = 0$ starts at 4.5 Ga).

We assume the number of bodies of water per unit area of continental crust is constant over time; thus, by multiplying Eq. **S1** by the number of lakes and ponds on Earth today, we get the number of bodies of water on Earth at any date from 4.5 Ga to 3.7 Ga. The number of lakes and ponds on Earth today (down to 0.001 km^2) is estimated to be 304 million (23); therefore, the equation becomes

$$N_t = 4.864 \times 10^7 t, \qquad \textbf{[S2]}$$

where N_t is the total number of bodies of water on Earth for times 0 Gy $\leq t \leq$ 0.8 Gy ($t = 0$ starts at 4.5 Ga).

Lake and Pond Size Distribution. The size distribution of lakes and ponds on Earth today follows a Pareto distribution function (23).

$$dN_A = N_t c k^c A^{-(c+1)} dA, \qquad \textbf{[S3]}$$

where dN_A is the number of bodies of water in the square kilometer area range A to $A + dA$, N_t is the total number of bodies of water on Earth, c is the dimensionless shape parameter, and k is the smallest lake/pond area in the distribution. The shape parameter was calculated for lakes and ponds down to 0.001 km^2 to be $c = 1.06$ (23).

The total area of ponds on Earth in a given size range can then be calculated by multiplying Eq. **S3** by A and integrating from A_{min} to A_{max}, which gives

$$A_{tot} = \frac{c}{-c+1} N_t k^c \left[A_{max}^{(-c+1)} - A_{min}^{(-c+1)}\right] \quad [\text{km}^2]. \qquad \textbf{[S4]}$$

There is an upper size limit on WLPs in which substantial concentrations of nucleobases from meteorites can be deposited. If the surface area of a WLP is comparable to the area of a meteoroid's strewnfield, then partial overlapping of the strewnfield and WLP is probable. This would lead to fewer fragment depositions per unit pond area, and lower nucleobase concentrations. For this reason, we choose the upper limit on WLP radii to be 10 m. This equates to pond areas that are <0.04% of the strewnfield area of typical carbonaceous meteoroids (the latter of which are ∼0.785 km^2).

There is also a lower size limit, as ponds that evaporate too quickly spend the majority of their time in the dry state. This would prevent nucleobase outflow from the pores of meteorites. Moreover, the probability of meteorite deposition in WLPs decreases for decreasing pond radii. A cylindrical WLP at 65 °C with a radius and depth of <1 m will likely evaporate in less than 3 mo without replenishment from rain or geysers (25). Therefore, we set the lower WLP radius and depth limit for our interests at 1 m.

Total WLP Surface Area. From Eqs. **S2** and **S4**, the total surface area of cylindrical, 1- to 10-m-radii WLPs on early Earth at time 0 Gy $\leq t \leq$ 0.8 Gy is

$$A_{tot}(t) = 651t \quad [\text{km}^2]. \qquad \textbf{[S5]}$$

For this calculation, we choose $c = 1.06$ and $k = 3.14 \times 10^{-6}$ km^2. Note that $t = 0$ starts at 4.5 Ga.

Calculating Carbonaceous Meteorite Depositions in WLPs

Aerodynamic forces fragment meteoroids that enter the atmosphere, which increases their total meteoroid cross-section, and thus their aerodynamic braking (32). Numerical simulations show that the fragments of carbonaceous meteoroids with initial diameters up to 80 m and atmospheric entry velocities near the median value [15 km/s (31)] reach terminal velocity (32). These fragments do not produce craters upon impact (49) and can be intactly deposited into WLPs. Larger meteoroids produce fragments with impact speeds too fast to avoid cratering and partial or complete melting or vaporization of the impactor. The same numerical simulations calculate the largest fragments from an 80-m-diameter carbonaceous meteoroid of initial velocity 15 km/s to be ∼20 cm in diameter (32). [This roughly makes sense, as the biggest carbonaceous meteorite recovered, the Allende, is only 110 kg—corresponding to a ∼40-cm-diameter sphere (50).]

The optimal diameter range for carbonaceous meteoroids to deposit a substantial fraction of mass into WLPs at terminal velocity is therefore 40 m to 80 m. We base our calculation of carbonaceous meteoroid fragment depositions on this range.

Mass Delivery Models. The lunar cratering record analyzed by the Apollo program has revealed a period of intense lunar bombardment from ∼3.9 Ga to 3.8 Ga (51). Whether a single lunar cataclysm (lasting ∼10 My to 150 My) or a sustained declining bombardment preceded 3.9 Ga is still debated (30). We choose three models for the rate of mass delivered to early Earth: an LHB model, and a minimum and a maximum bombardment model. All models are based on analyses of the lunar cratering record (6, 21).

Analyses from both dynamic modeling and the lunar cratering record estimate the total mass delivered to early Earth during

the LHB to be $\sim 2 \times 10^{20}$ kg (21). We assume that a Gaussian curve for the rate of impacts during the LHB (30), which centers on 3.85 Ga, integrates to 2×10^{20} kg, and drops to nearly zero at 3.9 and 3.8 Ga. Thus,

$$dm_{LHB}(t) = 5.33 \times 10^{21} e^{\frac{-(t-0.65)^2}{2(0.015)^2}} dt \quad \text{[kg]}, \qquad \textbf{[S6]}$$

where dm_{LHB} is the total mass from t to $t + dt$ (gigayears) (t = 0 starts at 4.5 Ga).

Equations for the minimum and maximum mass delivered to early Earth, given that a sustained declining bombardment preceded 3.9 Ga, are (6)

$$m_{minB}(t) = 1 \times 10^{21} - 0.76 \left[4.5 - t + 4.57 \times 10^{-7} \left(e^{(4.5-t)/\tau_a} - 1\right)\right] m_2^{1-b} 4\pi R_{moon}^2 \Sigma \quad \text{[kg]} \qquad \textbf{[S7]}$$

$$m_{maxB}(t) = 7 \times 10^{23} - 0.4 \left[4.5 - t + 5.6 \times 10^{-23} \left(e^{(4.5-t)/\tau_c} - 1\right)\right] m_2^{1-b} 4\pi R_{moon}^2 \Sigma \quad \text{[kg]}, \qquad \textbf{[S8]}$$

where m_{minB} and m_{maxB} are the total mass delivered from t = 0 to $t = t$ (t = 0 starts at 4.5 Ga), τ_a and τ_b are decay constants (τ_a = 0.22 Gy, τ_b = 0.07 Gy), m_2 is the maximum impactor mass ($m_2 = 1.5 \times 10^{18}$ kg), b = 0.47, R_{moon} is the mean radius of the moon (R_{moon} = 1737.1 km), and Σ is the ratio of the gravitational cross-sections of Earth and the moon ($\Sigma \sim 23$).

Taking the derivatives of Eqs. **S7** and **S8** gives us the corresponding rates of mass delivered to early Earth.

$$dm_{minB}(t) = 0.76 \left(1 + \frac{4.57 \times 10^{-7}}{\tau_a} e^{(4.5-t)/\tau_a}\right) m_2^{1-b} 4\pi R_{moon}^2 \Sigma dt \quad \text{[kg]}. \qquad \textbf{[S9]}$$

$$dm_{maxB}(t) = 0.4 \left(1 + \frac{5.6 \times 10^{-23}}{\tau_c} e^{(4.5-t)/\tau_c}\right) m_2^{1-b} 4\pi R_{moon}^2 \Sigma dt \quad \text{[kg]}. \qquad \textbf{[S10]}$$

See Fig. 1 for a plot of the three mass delivery models.

Impactor Mass Distribution. Chemical analyses of lunar impact samples, and crater size distributions, suggest that the impactors of Earth and the moon before ~3.85 Ga were dominated by main-belt asteroids (51). It is also likely that the size-frequency distribution of impactors on early Earth is similar to that of the main-belt asteroids today (52). Although there is no conclusive evidence to constrain the fraction of early Earth impactors that were of cometary origin, some suggest ~10% of the total accreted mass was from comets (6).

The early Earth impactor mass distribution for impactors with radii 20 m to 40 m, adjusted for the total mass delivered during the LHB, follows the linear relation

$$dm_{LHB}(r) = \left[7.5 \times 10^{13} r + 3 \times 10^{15}\right] dr \quad \text{[kg]}, \qquad \textbf{[S11]}$$

where dm is the mass of impactors with radii r to $r + dr$ (meters) (21).

To get the impactor mass distributions for the mass delivered between t and $t + dt$ in each of our three models, we multiply Eq. **S11** by Eq. **S6**, **S9**, or **S10**, and divide by 2×10^{20} kg.

$$dm_i(t, r) = \left[7.5 \times 10^{13} r + 3 \times 10^{15}\right] \frac{dm_i(t)}{2 \times 10^{20}} dr \quad \text{[kg]}, \qquad \textbf{[S12]}$$

where i is the model (LHB, minB, or maxB).

Impactor Number Distribution. Eq. **S12** can be turned into a number distribution (from t to $t + dt$) for asteroids of a specific size and type (e.g., carbonaceous chondrites, ordinary chondrites, irons) by multiplying by the fraction of impactors that are asteroids (f_a) and the fraction of asteroid impacts that are of a specific meteorite parent body type (f_t), and then dividing by the volume and average density of such asteroids. After simplification, this is

$$dN_i(t, r) = \frac{3 f_a f_t}{4\pi\rho} \left[\frac{7.5 \times 10^{13}}{r^2} + \frac{3 \times 10^{15}}{r^3}\right] \frac{dm_i(t)}{2 \times 10^{20}} dr, \qquad \textbf{[S13]}$$

where i is the model (LHB, minB, or maxB).

Total Number of Carbonaceous Impactors. Although some carbonaceous chondrites may have originated from comets (53), for this calculation, we conservatively assume that all carbonaceous meteorites originated from asteroids.

Integrating Eq. **S13** from r_{min} to r_{max} gives the total number of meteoroids in that radii range to have impacted early Earth, from t to $t + dt$, for each model.

$$dN_i(t) = \frac{3 f_a f_t}{4\pi\rho} \left[7.5 \times 10^{13} \left(\frac{1}{r_{min}} - \frac{1}{r_{max}}\right) + \frac{3 \times 10^{15}}{2} \left(\frac{1}{r_{min}^2} - \frac{1}{r_{max}^2}\right)\right] \frac{dm_i(t)}{2 \times 10^{20}}, \qquad \textbf{[S14]}$$

where i is the model (LHB, minB, or maxB).

Probability of WLP Deposition. The probability of an infinitesimally small object hitting within a target area, given that the probability of hitting anywhere within the total area is equal, is the geometric probability

$$P_g = \frac{A_{targ}}{A_{tot}}. \qquad \textbf{[S15]}$$

This equation can be used to estimate the probability of blindly hitting the bull's-eye on a dartboard from relatively close in, where A_{targ} is the area of the bull's-eye and A_{tot} is the area of the dartboard. In this case, since the tip of a dart is relatively small with respect to the bull's-eye, the approximation is relatively accurate. In the case of estimating the probability of meteoroid fragments falling into a WLP, the tip of the "dart" (i.e., the debris area of meteoroid fragments) is not always going to be larger than the "bull's-eye" (i.e., the total surface area of WLPs at any time). For example, the probability of fragments from a single meteoroid falling into a WLP at ~4.5 Ga to 4.45 Ga, when there was a small fraction of continental crust and few WLPs, is more analogous to the probability of blindly hitting the bull's-eye with a small ball, which would be slightly more likely than with a dart. Any large enough part of the ball overlapping with the bull's-eye counts as a hit, as does any large enough part of the debris field overlapping with the combined WLP surface area. "Large enough," in our case, corresponds to the area of the largest WLP for which the meteoroid fragment deposition probability is being calculated (or, equivalently, 100 of the smallest WLPs in our study). (This minimum area is necessary to assume a homogeneous surface deposition when calculating the total mass of meteoroid fragments to have entered a WLP.)

To use Eq. **S15** to calculate the probability for the fragments of a single meteoroid landing in a primordial WLP, A_{targ} must be the effective target area. The effective target area is illustrated in Fig. S6. Any meteoroid that enters the atmosphere within the effective target area (of radius d) disperses its fragments over at least one WLP's entire surface.

The area of the asymmetric "lens" in which any two circles intersect is

$$A = r^2 cos^{-1}\left(\frac{d^2 + r^2 - R^2}{2dr}\right) + R^2 cos^{-1}\left(\frac{d^2 + R^2 - r^2}{2dR}\right) - \frac{1}{2}\sqrt{(-d + r + R)(d + r - R)(d - r + R)(d + r + R)}, \quad \textbf{[S16]}$$

for circles of radii r and R, and distance between their centers d (54).

In Fig. S6, the asymmetric lens created by the intersection of the combined WLP surface area at a given time and the meteoroid fragment debris area corresponds to the area of the largest individual WLP in our distribution. Because the effective target area radius, d, grows linearly with total WLP surface area radius, R, we can plot Eq. **S16** at $t = 1$ Gy to solve for d, and input the linear time dependence afterward. For this calculation, $A = 3.14 \times 10^{-4}$ km^2, $r = r_g = 0.5$ km, and $R = \sqrt{651 \text{ km}^2/\pi} = 14.4$ km. This gives us the effective target radius, $d = 14.9$ km, and corresponds to an effective target area,

$$A_{eff}(t) = 697t \quad [\text{km}^2]. \quad \textbf{[S17]}$$

See Fig. 1 for a plot of the effective WLP surface area over time.

Finally, the probability of the fragments from all CM-, CI-, or CR-type meteoroids (Mighei type, Ivuna type, and Renazzo type, respectively) with radii $r_{min} = 20$ m to $r_{max} = 40$ m landing in WLPs on early Earth of radii 1 m to 10 m from time t to $t + dt$ is the product of Eqs. **S14** and **S15**.

$$dP_i(t) = \frac{697t}{4\pi R_\oplus^2} dN_i(t), \quad \textbf{[S18]}$$

where i is the model (LHB, minB, or maxB).

In Fig. S7, we plot the normalized probability distributions (dP_i/dt) for the deposition of carbonaceous meteorites into WLPs from 4.5 Ga to 3.7 Ga. The LHB, the minimum bombardment, and the maximum bombardment models are compared. For the LHB model, there are 10 WLP depositions from 3.9 Ga to 3.8 Ga; 95% of these depositions occur between 3.88 and 3.82 Ga. For the minimum bombardment model, there are 15 WLP depositions during the entire Hadean Eon; however, 95% of these depositions occur between 4.47 and 3.77 Ga. Finally, for the maximum bombardment model, there are 3,840 depositions during the Hadean Eon, with 95% of these depositions occurring between 4.50 and 4.17 Ga. See Fig. 1 for cumulative deposition distributions.

One assumption is made in our deposition probability calculation, which is, given that the largest WLP considered is completely within the carbonaceous meteoroid's strewnfield, at least one fragment will land in the WLP. (An equivalent assumption would be, given that 100 of the smallest WLPs considered are completely within the meteoroid's strewnfield, at least one fragment will deposit into one of the ponds.) To determine whether this is the case, we need a good estimate for the number of fragments that spread over a debris field from a single carbonaceous meteoroid. For the Pułtusk stony meteoroid, which entered Earth's atmosphere above Poland in 1868 (55), the number of fragments is estimated to be 180,000 (55). Although the Pułtusk meteorites may not represent the typical fragmentation of stony meteoroids, since this meteoroid is about 1.6 times denser than the average carbonaceous meteoroids in our study (56), we would expect a carbonaceous meteoroid to fragment more than the typical stony meteorite. If meteoroid fragments are randomly spaced within a strewnfield, then Eq. **S15** multiplied by the number of meteoroid fragments will give us roughly the number of fragments that will enter a WLP. (In this case, A_{targ} is the area of the cylindrical pond, and A_{tot} is the area of the strewnfield.). From this calculation, given that a 10-m-radius WLP is within a 180,000-fragment strewnfield of radius 500 m, roughly 72 carbonaceous meteoroid fragments will land in the pond. In fact, as long as 40- to 80-m carbonaceous meteoroids fragment into at least 2,500 pieces, fragment deposition into a 10-m-radius WLP is probable. We therefore consider this assumption reasonable.

Sensitivity Analysis. In our estimate of the number of carbonaceous meteoroids that led to WLP depositions on early Earth, we assume that, from 4.5 Ga to 3.7 Ga, the continental crust grows at 16%/Gy (29), and the ponds per unit area is the same as today. However, the uncertainty in the growth rate of continental crust and the WLPs per unit area on early Earth is high. For example, the number of WLPs per unit area was probably higher on the above-sea-level crust of the Hadean Earth than it is on Earth's continents now. The greater rate of asteroid bombardment during the Hadean (30) would have created many small craters, which, over a few rain cycles, could fill to become ponds. On the other hand, geophysical models suggest the surface ocean was increasing in volume from ~4.5 Ga to 4.0 Ga (57). This would slow the growth rate of above-sea-level crust. Because of these uncertainties, we adjust the growth rate of WLPs on early Earth by plus or minus one order of magnitude to obtain error bars. Because the probability of deposition (Eq. **S18**) is directly proportional to the number of WLPs on early Earth, varying the growth rate of WLPs by plus or minus one order of magnitude equates to a plus or minus one order of magnitude uncertainty in the WLP deposition expectation values (Fig. 1).

Sources and Sinks Model Overview

Calculating the water and nucleobase content in WLPs over time is a problem of sources and sinks. These sources and sinks are illustrated in Fig. 2 and displayed in Table S1.

Because nucleobase diffusion from carbonaceous meteorite fragments is slow (*Nucleobase Outflow and Mixing*), this source is only turned on in the wet phase. Although it may be possible for nucleobases to occasionally enter WLPs from runoff, we do not consider this as a source. IDPs that fall on dry land are the most likely nucleobase source to be carried by runoff into WLPs (because of their low mass). However, these IDPs are exposed to photodissociating UV light until they are picked up by a runoff stream, by which time few if any enclosed nucleobases likely remain. Hydrolysis of nucleobases only occurs in the presence of liquid water; therefore, we only turn on this sink when our ponds are wet. Similarly, seepage of nucleobases through the pores in the bases of WLPs only occurs during the wet phase. A 1-m column of pond water can absorb UV radiation up to ~95% (37); therefore, as a first-order approximation, we only turn on UV photodissociation when our WLPs are in the dry phase. We do not consider cosmic rays as a sink for nucleobases, as a study has shown that adenine has a half-life of millions of years from cosmic ray dissociation at 1 AU (58). This is several orders of magnitude greater than the timescales of nucleobase decay from the other sinks. Finally, since we are interested in accumulating nucleobases in WLPs so that they can react to form nucleotides, a future model will include such reactions as a sink.

Pond Water Sources and Sinks

Evaporation. There are many variables that could go into a pond evaporation calculation. However, a simple relation was obtained by measuring the depth and temperature of a ~1-m-radius lined pond (to prevent seepage) and a class-A cylindrical evaporation pan over time,

$$\frac{dE}{dt} = -9.94 + 5.04T \quad [\text{mm·mo}^{-1}], \quad \textbf{[S19]}$$

where dE is the drop in pond depth, and T is the pond temperature in degrees Celsius (25).

This relation is converted to meters per year,

$$\frac{dE}{dt} = -0.12 + 0.06\,T \quad [\mathrm{m{\cdot}y^{-1}}]. \qquad \textbf{[S20]}$$

Seepage. Unless the material (e.g., basalt, soil, clay) at the base of a WLP is saturated in water, gravity will cause pond solution to seep through the pores in this material. The average seepage rate of 55 small ponds in Auburn, Ala., was measured to be 5.1 $\mathrm{mm{\cdot}d^{-1}}$ (26). This value is high compared with the average seepage rates from small ponds in North Dakota and Minnesota (1.0 $\mathrm{mm{\cdot}d^{-1}}$) and the Black Prairie region of Alabama (1.6 $\mathrm{mm{\cdot}d^{-1}}$) (26). These seepage rates are comparable in magnitude to the pond evaporation rates in *Evaporation*, and therefore must be considered as a sink for water and nucleobases in our WLP model. We take an average of the above three values and apply a constant seepage rate of 2.6 $\mathrm{mm{\cdot}d^{-1}}$ to our WLP water evolution calculations.

$$\frac{dS}{dt} = 0.95 \quad [\mathrm{m{\cdot}y^{-1}}]. \qquad \textbf{[S21]}$$

We assume that the majority of seepage occurs from the base of the pond, where the water pressure is the highest. The effect of seepage on nucleobase mass loss is handled in *Nucleobase Sinks*.

Precipitation. If we ignore the possibility of local water geysers, the main source of pond water is likely to be precipitation. It has been shown that the vast majority of monthly precipitation climates around the world can be adequately described by a sinusoidal function with a 1-y period (24). That is,

$$\frac{dP}{dt} = \overline{P}\left[1 + \delta_p sin\left(\frac{2\pi(t - s_p)}{\tau_s}\right)\right] \quad [\mathrm{m{\cdot}y^{-1}}], \qquad \textbf{[S22]}$$

where dP is the amount of precipitation, $\overline{P}$ is the mean precipitation rate (meters per year), δ_p is the dimensionless seasonal precipitation amplitude, s_p is the phase shift of precipitation (years), t is the time (years), and τ_s is the duration of the seasonal cycle (i.e., 1 y) (24).

From 1980 to 2009, the mean precipitation on Earth ranged from ∼0.004 $\mathrm{m{\cdot}y^{-1}}$ to 10 $\mathrm{m{\cdot}y^{-1}}$ (with a global mean of ∼0.7 $\mathrm{m{\cdot}y^{-1}}$), the seasonal precipitation amplitudes ranged from ∼0 to 4.7, and the latitude-dependent phase shift ranged from 0 y to 1 y (24).

Summary. The evaporation and seepage rates minus the rate of water rise due to precipitation gives us the overall rate of water decrease in a WLP.

$$\frac{dL}{dt} = 0.83 + 0.06\,T - \overline{P}\left[1 + \delta_p sin\left(\frac{2\pi(t - s_p)}{\tau_s}\right)\right] \quad [\mathrm{m{\cdot}y^{-1}}]. \qquad \textbf{[S23]}$$

Eq. **S23** is too complex to be solved by standard analytical techniques or mathematical software; therefore, we solve it numerically using a forward time finite difference approximation with the boundary conditions $0 \le L(T, t) \le r_p$. We then convert the drop in pond depth as a function of time, $L(t)$, to the mass of water in the WLP using the water density and the volume of a cylindrical portion. This equates to

$$m(t) = \pi\rho_w r_p^2(r_p - L) \quad [\mathrm{kg}]. \qquad \textbf{[S24]}$$

For our models, we assume pond water of density ρ_w = 1,000 $\mathrm{kg{\cdot}m^{-3}}$.

Nucleobase Sinks

Hydrolysis. The first-order hydrolysis rate constants for adenine (A), guanine (G), uracil (U), and cytosine (C) have been measured from decomposition experiments at pH 7 (28). These rate constants are expressed in the Arrhenius equations,

$$k_A = 10^{\frac{-5902}{T} + 8.15} \qquad \textbf{[S25]}$$

$$k_G = 10^{\frac{-6330}{T} + 9.40} \qquad \textbf{[S26]}$$

$$k_U = 10^{\frac{-7649}{T} + 11.76} \qquad \textbf{[S27]}$$

$$k_C = 10^{\frac{-5620}{T} + 8.69} \quad [\mathrm{s^{-1}}]. \qquad \textbf{[S28]}$$

The nucleobase decomposition rate due to being dissolved in water can then be obtained by plugging Eqs. **S25–S28** into the first-order reaction rate law,

$$\frac{dm_i}{dt} = -m_i\gamma k \quad [\mathrm{kg{\cdot}y^{-1}}], \qquad \textbf{[S29]}$$

where γ = 3,600 · 24 · 365.25 $\mathrm{s{\cdot}y^{-1}}$.

The hydrolysis rates of adenine, guanine, and cytosine remain relatively stable in solutions with pH values from 4.5 to 9 (28, 59). WLPs may have been slightly acidic (from pH 4.8 to 6.5) due to the higher partial pressure of CO_2 in early Earth atmosphere (34).

UV Photodissociation. The photodestruction of adenine has been studied by irradiating dried samples under Martian surface UV conditions (27). This quantum efficiency of photodecomposition (from 200 nm to 250 nm)—which is independent of the thickness of the sample—was measured to be $1.0 \pm 0.9 \times 10^{-4}$ molecules per photon (27).

For the calculation of the quantum efficiency of adenine, a beam of UV radiation was focused on a thin compact adenine sample formed through sublimation and recondensation (27). In this case, all of the photons in the beam of UV radiation were incident on the nucleobases. In the WLP scenario, not all of the incoming UV photons will be incident on nucleobases. Instead, large gaps can exist between nucleobases that collect at the base of the pond. Therefore, the number of photons incident on the pond area is not the same as those incident on the scattered nucleobases unless there are at least enough nucleobases present to cover the entire pond area. Since the nucleobases are mixed well into the pond water before complete evaporation, we assume nucleobases will spread out evenly as they collect on the base of the pond. This means we assume that all locations on the base of the pond are covered in nucleobases before nucleobases stack on top of one another. For low abundances of total nucleobases in a WLP, this approach will lead to a slightly higher estimate for the rate of photodissociation than expected. We deem this acceptable for a first-order estimate of nucleobase photodissociation.

The mass of nucleobases photodestroyed per year, per area covered by nucleobases (i.e., the photodestruction flux), is constant over time and is dependent on the experimentally measured quantum efficiency of photodecomposition.

$$\dot{M}_i = \frac{\Phi F\lambda\gamma\mu_i}{hcN_A} \quad [\mathrm{kg{\cdot}y^{-1}\cdot m^{-2}}], \qquad \textbf{[S30]}$$

where Φ is the quantum efficiency of photodecomposition of the molecules (molecules per photon), F is the UV flux incident on the entire pond area (watts per square meter), λ is the average wavelength of UV radiation incident on the sample (meters), γ is 3,600 · 24 · 365.25 $\mathrm{s{\cdot}y^{-1}}$, μ_i is the molecular weight of the irradiated molecules (kilograms per mole), h is Planck's constant (kilogram square meters per second), c is the speed of light (meters per second), and N_A is Avogadro's number (molecules per mole).

Our estimation of the photodestruction rate of a nucleobase depends on the total mass of the nucleobase within the WLP. If there is enough of the nucleobase present for the entire base of the pond to be covered, we can multiply the photodestruction flux by the entire pond area. Otherwise, we must multiply the photodestruction flux by the combined cross-sectional area of the nucleobase present in the WLP to get the photodestruction rate.

$$\frac{dm_i}{dt} = \begin{cases} -\dot{M}_i \dfrac{m_i}{\rho_i d}, & \text{if } \dfrac{m_i}{\rho_i d} < A_p \\ -\dot{M}_i A_p, & \text{otherwise} \end{cases} \quad [\text{kg}\cdot\text{y}^{-1}], \qquad \textbf{[S31]}$$

where m_i is the mass of the sample (kilograms), ρ_i is the mass density of the nucleobase (kilograms per cubic meter), d is the distance between two stacked nucleobases in the solid phase (meters), and A_p is the area of the WLP (square meters).

Assuming cloudless skies, an upper limit on early Earth integrated UV flux from 200 nm to 250 nm is $\sim$0.4 W·m^{-2} (36, 60). UV wavelengths of $<$200 nm would be completed attenuated by CO_2 and H_2O in the early atmosphere (36). The mass density of solid adenine is 1,470 kg·m^{-3}, making the distance between two stacked adenine molecules in the solid phase $\sim$6.6 Å. For guanine, uracil, and cytosine, we take the mass densities to be 2,200, 1,320, and 1,550 kg·m^{-3}, respectively.

Seepage. The constant pond water seepage $\dot{S} = 0.95$ m·y^{-1} was determined in *Pond Water Sources and Sinks*. This can be used to calculate the nucleobase seepage rate via the equation

$$\frac{dm_i}{dt} = w_i \rho_w A_p \dot{S} \quad [\text{kg}\cdot\text{y}^{-1}], \qquad \textbf{[S32]}$$

where w_i is the nucleobase mass fraction, ρ_w is the density of water (kilograms per year), and A_p is the area of the WLP (square meters).

Nucleobase Outflow and Mixing

Chondritic IDPs and meteorites are porous (61–63). With the exception of the nucleobases potentially formed due to surface photochemistry (12), any soluble nucleobases delivered to prebiotic Earth by carbonaceous IDPs and meteorites would have lain frozen in the pores of these sources upon their entering the atmosphere. Pulse heating experiments show that approximately $\sim$1 to 6% of the organics within IDPs could have survived atmospheric entry (62). In addition, based on their presence in carbonaceous chondrites today, nucleobases in carbonaceous meteorites evidently would have also survived atmospheric entry heating. Therefore, both sources, upon entering WLPs on prebiotic Earth, would have slowly released their remaining soluble nucleobases into the surrounding pond water. These nucleobases would then slowly homogenize into the pond solution.

We model the outflow of nucleobases from carbonaceous IDPs and meteorites and the mixing of a local concentration of nucleobases into a WLP using finite difference approximations of the one-dimensional advection–diffusion equation (see *Advection and Diffusion Model* for complete details).

Our model of nucleobase outflow is run for average-sized IDPs ($r = 100$ μm), and for small ($r = 1$ cm), medium ($r = 5$ cm), and large ($r = 10$ cm) carbonaceous meteorites. The fraction of nucleobases remaining in each of these sources as a function of time is plotted in Fig. S4.

Our models show that the duration of nucleobase diffusion from carbonaceous IDPs and meteorites into WLPs is mostly determined by the radius of the source. For typical, 100-μm-radius carbonaceous IDPs lying at the bottom of a WLP, it takes $<$2 min for $>$99% of the soluble nucleobases to diffuse into the surrounding pond water. For 1-cm-radius carbonaceous meteorites, this time increases to 10 d. For the largest carbonaceous meteoroid fragments, with radii of 5 cm and 10 cm, this duration increases to $\sim$8 and 32 mo, respectively.

For nucleobase mixing, we model a base-to-surface convection cell within cylindrical ponds with equal radii and depths of 1 m, 5 m, and 10 m. This model gives us the timescale of mixing a local concentration of nucleobases within WLPs. The maximum percent local nucleobase concentration difference from the average is plotted as a function of time in Fig. S8. This metric allows us to characterize the nucleobase homogeneity in a convection cell of the WLP.

Our simulations suggest that the mixing of local deposits of nucleobases in WLPs, resulting from their diffusion out of carbonaceous IDPs and meteorites, is a very efficient process. For a cylindrical WLP 1 m in depth, it will take about 35 min for a local deposition to homogenize in a convection cell within the pond. For larger WLPs, with 5- and 10-m depths, the nucleobase mixing time increases to 104 and 150 min, respectively. These short mixing times make it clear that, for carbonaceous meteorites $\geq$ 1 cm in radius, nucleobase homogenization in WLPs is dominated by the nucleobase outflow time from these bodies. In contrast, being that carbonaceous IDPs are much smaller than meteoroid fragments, the nucleobase outflow time from IDPs is negligible compared with the nucleobase homogenization time in WLPs.

Nucleobase Evolution Equation from IDPs

It is estimated that, at 4 Ga, approximately 6×10^8 kg·y^{-1} of carbonaceous IDPs were being accreted onto Earth (11). Since IDPs are tiny (typically $\sim$100 μm in radius), they are circulated by the atmosphere upon accretion and thus likely reached almost everywhere on prebiotic Earth. Approximately 1 to 6% of the organic content within IDPs could have survived the pulse heating of atmospheric entry (62). Assuming IDPs accreted uniformly, the surface nucleobase mass accretion per square area would be

$$\frac{dm_i}{dtdA} = \frac{w_i \dot{m}_I f_s}{4\pi R_\oplus^2} \quad [\text{kg}\cdot\text{y}^{-1}\cdot\text{m}^{-2}], \qquad \textbf{[S33]}$$

where w_i is the nucleobase mass fraction within IDPs for nucleobase i, $\dot{m}_I$ is the mass accretion rate of IDPs on prebiotic Earth (kilograms per year), and f_s is the average fraction of nucleobases that survive pulse heating from atmospheric entry.

IDPs are thought to correspond to origins of asteroids or comets (11); therefore, at best, the average nucleobase abundances in IDPs could match the average nucleobase content within the nucleobase-rich CM, CR, and CI meteorites. The average abundances of adenine, guanine, and uracil in CM, CR, and CI meteorites are listed in Table S2, along with the weighted averages based on relative fall frequencies. These abundances might be an upper limit for the guanine, adenine, and uracil content of IDPs, because, unlike the interior of large meteorites, molecule-dissociating UV radiation can penetrate everywhere within micrometer-to-millimeter-sized pieces of dust.

The amount of cytosine that could have formed on the surfaces of primordial IDPs is not well constrained. Cytosine has been detected in experiments exposing IDP analogs to UV radiation, but hasn't been quantified (12). Furthermore, these analog experiments formed cytosine via photoreactions involving pyrimidine: a molecule that has no measured abundance in IDPs or meteorites. For this analysis, we explore a best-case scenario, and set the maximum cytosine IDP abundance to 141.3 ppb (the possible upper limit of guanine in carbonaceous IDPs).

In *Nucleobase Outflow and Mixing*, we learned that nucleobase diffusion from IDPs is quick (lasting $<$2 min), and nucleobase homogenization in WLPs takes 1 h to a few hours, depending on the pond size. If we spread out the 6×10^8 kg·y^{-1} accretion rate of IDPs uniformly across the surface of Earth—assuming

IDPs are all 100-μm-radius spheres of CI, CM, and CR type (ρ = ~2,185 kg·m^{-3})—then IDPs would drop into 1- to 10-m-radius primordial WLPs at approximately 0.05 h^{-1} to 5 h^{-1}. Since each carbonaceous IDP can only carry a tiny mass in nucleobases (~1 pg), nucleobase inhomogeneities within WLPs would be a maximum of ~15 pg. This abundance of nucleobases is negligible; therefore, for our calculations of nucleobase accumulation in WLPs from IDP sources, we can assume that nucleobase deposition and pond homogenization are instantaneous.

Thus, the differential equation for the mass of nucleobase i accumulated in a WLP from IDP sources over time is the sum of the nucleobase mass accretion rate from IDPs, the nucleobase mass decomposition rate, the nucleobase mass seepage rate, and the nucleobase photodissociation rate,

$$\frac{dm_{i,IDP}(t)}{dt} = \frac{w_i \dot{m}_I f_s A_p}{4\pi R_\oplus^2} - \gamma m_i k_i - w_i \rho_w A_p \dot{S} - \begin{cases} \dot{M}_i \dfrac{m_i}{\rho_i d}, & \text{if } \dfrac{m_i}{\rho_i d} < A_p \\ \dot{M}_i A_p, & \text{otherwise} \end{cases} \quad [\text{kg·y}^{-1}]. \qquad \textbf{[S34]}$$

The second and third terms after the equal sign are only activated when the pond is wet, and the fourth term is only activated when the pond is dry. The first term is always activated, as recently accreted nucleobases are susceptible to UV dissociation while still lying in the pores of IDPs, and they effectively instantaneously outflow from IDPs upon wetting.

Using Eq. **S34**, we compute the nucleobase mass as a function of time numerically using a forward time finite difference approximation. We then divide the nucleobase mass by the water mass at each time step to obtain the nucleobase mass concentration over time. Because some ponds are seasonally dry, we freeze the water level at 1 mm during the dry phase to calculate a nucleobase concentration during this phase.

Nucleobase Evolution Equation from Meteorites

Simulations show that the fragments from carbonaceous meteoroids with diameters from 40 m to 80 m and initial velocities of 15 km/s will expand over a radius of ~500 m, and ~ 32% of the original meteoroids will survive ablation (32). Since a single meteoroid impacting the atmosphere may break up into 180,000 fragments before spreading across its strewnfield, it is probable that a meteorite deposition event involves multiple meteorites landing in a single WLP. The best estimate of the total nucleobase mass deposited into a WLP is thus calculated assuming the ablated meteoroid mass is spread uniformly over its strewnfield. Considering this, the total nucleobase mass to deposit into a WLP from a meteoroid would be

$$m_{i0} = \frac{4}{3} \frac{w_i f_s r^3 \rho A_p}{r_g^2} \quad [\text{kg}], \qquad \textbf{[S35]}$$

where w_i is the nucleobase mass fraction within the meteoroid for nucleobase i, f_s is the fraction of the meteoroid to survive ablation, r is the meteoroid radius as it enters Earth's atmosphere (meters), ρ is the density of the meteoroid (kilograms per cubic meter), r_g is the radius of the debris when the meteoroid fragments hit the ground (meters), and A_p is the area of the WLP (square meters).

After the deposition of meteoroid fragments into a WLP, the frozen meteorite interiors will thaw to pond temperature, allowing hydrolysis to begin inside the fragments' pores. This means the total mass of nucleobases that diffuse from the fragments' pores into the pond will be less than the total initial nucleobase mass within the deposited fragments. By integrating the nucleobase hydrolysis rate (Eq. **S29**), we obtain the mass of nucleobase i remaining after a given time of hydration t_h,

$$m_i = m_{i0} e^{-\gamma k_i t_h} \quad [\text{kg}]. \qquad \textbf{[S36]}$$

Note that t_h (years) may be different from t, as the hydration clock is paused when WLPs are dry.

Unlike carbonaceous IDPs, which unload their nucleobases into a WLP in seconds, nucleobases may not completely outflow from all deposited carbonaceous meteoroid fragments before the WLP evaporates. (However, the nucleobases that do outflow from the meteorites will mix homogeneously into the WLP within a single day–night cycle.) Thus, we calculate the nucleobase outflow time constants for 1-, 5-, and 10-cm-radius carbonaceous meteorites by performing least-squares regressions of our nucleobase diffusion simulation results to the function

$$f(t_h) = \alpha \left(1 - e^{-\frac{t_h}{\tau_d}}\right). \qquad \textbf{[S37]}$$

This equation shows that, as time increases, the mass of nucleobases that have flowed out of a single meteorite, into the WLP, approaches the coefficient α—which represents the total initial nucleobase mass contained in the meteorite. Since nucleobase outflow is mass-independent, we can use an arbitrary initial total nucleobase mass for α in our simulations to obtain the nucleobase outflow time constants.

The results of the fits give diffusion time constants for 1-, 5-, and 10-cm-radius fragments of $\tau_d = 4.9 \times 10^{-3}$ y, 0.12 y, and 0.48 y, respectively.

Adding up the sources and sinks gives us the nucleobase mass within the WLP from meteorite sources as a function of time and hydration time.

$$\frac{dm_{i,Met}(t,t_h)}{dt} = \frac{m_{i0}}{\tau_d} e^{-t_h\left(\gamma k_i + \frac{1}{\tau_d}\right)} - \gamma m_i k_i - w_i \rho_w A_p \dot{S} - \begin{cases} \dot{M}_i \dfrac{m_i}{\rho_i d}, & \text{if } \dfrac{m_i}{\rho_i d} < A_p \\ \dot{M}_i A_p, & \text{otherwise} \end{cases} \quad [\text{kg·y}^{-1}]. \qquad \textbf{[S38]}$$

The first three terms after the equal sign are only activated when the pond is wet, and the fourth term is only activated when the pond is dry.

Since there are many possibilities for the sizes of meteoroid fragments that will enter a WLP, we consider three simplified models: All fragments that enter a WLP from a meteoroid of radius 20 m to 40 m are either 1 cm in radius, 5 cm in radius, or 10 cm in radius. These three models represent a local part of the strewnfield that deposited either many small fragments, mostly medium-sized fragments, or just a couple to a few large fragments.

Cytosine is unlikely to have sustained within meteorite parent bodies long enough to be delivered to early Earth by meteorites (15); therefore, we only model the accumulation of adenine, guanine, and uracil in WLPs from meteorite sources.

We solve Eq. **S38** numerically using a forward time finite difference approximation. Nucleobase concentration is then obtained by dividing the nucleobase mass by the water mass in the WLP at each time step.

Additional Results

Pond Water. In Fig. S9, we explore the effects of changing temperature on wet environment WLPs of 1-m radius and depth (see Table 1 for wet environment model details). To do this, we vary our fiducial model temperatures (65 °C for a hot early Earth and 20 °C for a warm early Earth) by ±15 °C. As temperature increases, evaporation becomes more efficient; however, the wet environment WLPs never dry completely.

Nucleobase Accumulation from IDPs. In Fig. S1, we explore the evolution of adenine concentration from only IDP sources in WLPs of 1-m radius and depth. We model the adenine accumulation in three environments (dry, intermediate, and wet) on a

hot and warm early Earth (see Table 1 for precipitation model details). Fig. S1*A* is for 65 °C on a hot early Earth and 20 °C on a warm early Earth, and Fig. S1*B* is for 50 °C on a hot early Earth and 5 °C on a warm early Earth.

All adenine concentration curves reach a stable seasonal pattern within ∼5 y. The highest adenine concentrations occur for models with a dry phase (i.e., the dry and intermediate models at 65 °C, and the dry model at 50 °C.) The lower maximum concentrations in the models without a dry phase are due to the sustained high water levels. The maximum adenine to accumulate in any model from IDP sources is ∼0.2 ppq. This occurs just before the pond dries. Upon drying, UV photodissociation immediately drops the adenine concentration to an amount which balances the incoming adenine from IDP accretion. The curves in Fig. S1 do not change drastically with increasing pond radius and depth once a stable seasonal pattern is reached. This is because, although ponds of increasing surface area collect more nucleobases, these ponds have an equivalent increase in area to nucleobase seepage.

In Fig. S2, we explore guanine, uracil, and cytosine accumulation in degenerate dry environment WLPs for a hot early Earth at 65 °C and a warm early Earth at 20 °C (see Table 1 for details). The differences in each nucleobase mass fraction over time are caused by the different initial abundances of each nucleobase in IDPs (Table S2). Although hydrolysis rates differ between nucleobases, decay due to hydrolysis is negligible over <10-y periods at temperatures lower than ∼70 °C.

In Fig. S5, we turn off seepage, e.g., resembling a scenario where a lipid biofilm has covered the WLP base, and explore the evolution of adenine concentrations from IDP sources. This model is displayed for a hot early Earth at 65 °C and a warm early Earth at 20 °C (see Table 1 for details). UV photodissociation is always the dominant nucleobase sink for the dry and intermediate environments; therefore, for this model, we only display the evolution of adenine in the wet environment, where hydrolysis takes over as the dominant nucleobase sink.

In the absence of seepage, adenine concentrations can build up in wet environment WLPs until the rate of incoming adenine from IDPs matches the decay rate due to hydrolysis. Hydrolysis rates are faster at hotter temperatures; therefore, maximum adenine concentrations are higher and take longer to converge in the 20 °C pond compared with the 65 °C pond. However, these maximum adenine concentrations are 145 and 0.3 ppq, respectively, which are negligible in comparison with the parts per billion–parts per million-level adenine concentrations reached in WLPs from carbonaceous meteorite sources.

Nucleobase Accumulation from Meteorites. In Fig. S10, we explore the evolution of adenine concentrationin WLPs with radii and depths of 1 m, from 1-cm fragments of an initially 40-m-radius carbonaceous meteoroid. The models correspond to degenerate environments on a hot (65 °C) and warm (20 °C) early Earth. The maximum adenine concentration in the intermediate environment is ∼1.4 ppm, and occurs 16 h after the fragments deposit into the nearly empty pond. The dry and wet environments allow for a maximum adenine concentration of ∼2 ppm. Because adenine outflow from 1-cm-sized meteorites occurs in just 10 d, only adenine sinks exist from 10 d onward. As the ponds wet, the adenine concentrations decrease exponentially, and, as the ponds dry again, the curves flatten out and ramp up slightly before the ponds completely dry up. When the ponds dry, UV radiation quickly wipes out the adenine at the base of the ponds. Since the wet environment doesn't have a dry phase, the adenine concentration slowly diminishes in this model, due mainly to seepage.

The adenine mass fraction curves in Fig. S10, over a 2-y period, do not change, as pond radii and depths increase equally. This is because, although the mass of water in a WLP increases for larger collecting areas, larger pond areas also collect more meteorite fragments, which counterbalances the water mass and keeps the nucleobase concentration the same.

In Fig. S11, we explore how initial meteoroid radius affects the maximum concentration of adenine accumulated (from its fragments) in WLPs with radii and depths of 1 m. The maximum adenine concentration only differs by at most a factor of 8 when varying the initial meteoroid radius from 20 m to 40 m. This is because the nucleobase mass to enter a WLP scales with the meteoroid mass, i.e., $\propto r^3$.

Finally, in Fig. S3, we explore guanine and uracil accumulation in intermediate and wet environment WLPs with radii and depths of 1 m. These models correspond to a hot early Earth at 65 °C and a warm early Earth at 20 °C. The small differences between each nucleobase mass fraction over time are due to the different initial nucleobase abundances in the deposited meteorite fragments (Table S2). Although each nucleobase has a different hydrolysis rate (Eq. **S25**), the decay of guanine, adenine, and uracil due to hydrolysis is negligible in <10 y for temperatures of <65 °C.

Advection and Diffusion Model

Advection and diffusion are the two main considerations of solute transport in water. Because nucleobases will diffuse out of the pores of carbonaceous IDPs and meteorites at a different rate than they will mix homogeneously in the WLP, we separate our nucleobase transport model into two distinct parts. In part one, we model the outflow of nucleobases from carbonaceous IDPs and meteorites. In part two, we model the mixing of a local concentration of nucleobases into a WLP.

Both parts of our simulation can be modeled with the advection–diffusion equation below, with either one or both right-hand side terms "turned on."

$$\phi\frac{\partial C_i}{\partial t} = \nabla\cdot[D_{eff}\nabla C_i] - \nabla\cdot[uC_i], \qquad \textbf{[S39]}$$

where ϕ is the porosity of the medium, C_i is the mass concentration of the species, D_{eff} is the effective diffusion coefficient (often in square meters per second), and u is the convective fluid velocity (64).

For a 1D case, where the diffusion coefficient and fluid velocity are constant along the simulated path, the advection–diffusion equation can be written as

$$\phi\frac{\partial C_i}{\partial t} = D_{eff}\frac{\partial^2 C_i}{\partial r^2} - u\frac{\partial C_i}{\partial r}. \qquad \textbf{[S40]}$$

For part one of our nucleobase transport model (the nucleobase outflow portion), we set $u = 0$. This is because carbonaceous IDPs and meteoroid fragments are likely too small to attain noticeable interior pressure differences (thus the convective velocity within these bodies is probably negligible).

We do not consider hydrolysis in our nucleobase transport model, as we only intend on estimating nucleobase outflow and mixing timescales from these models (rather than the nucleobases remaining after these processes). Since nucleobase decay is uniform within the carbonaceous sources and WLPs, and is also very slow at WLP temperatures [$t_{1/2}$ is approximately tens to hundreds of years (15)], it is not likely to affect the timescales of complete nucleobase outflow from the source or homogenization within the WLP. A nonzero amount of nucleobases will decompose during diffusion from the source, and during mixing within the WLP. However, this is considered in the final calculations of nucleobase accumulation within WLPs from each source (see *Nucleobase Evolution Equation from IDPs* and *Nucleobase Evolution Equation from Meteorites*).

The advection–diffusion equation also does not include adsorption or formation reactions. However, for the diffusion of soluble nucleobases from small porous environments which previously reached chemical equilibrium, the effects of these extra

sources and sinks will probably be minimal. Also, to adjust the diffusion equation for a free water medium, one simply needs to set $\phi = 1$, and $D_{eff} = D_{fw}$.

The effective diffusion coefficient of a species is proportional to, but smaller than, its free water diffusion coefficient. Many equations exist for modeling the effective diffusion coefficient in porous media (65–68). These equations depend on variables such as the porosity, tortuosity, and constrictivity of the medium, which represent the void space fraction, the curves in the pores, and the bottleneck effect, respectively. These equations are listed in Table S3.

Carbonaceous meteorites of type CM, CR, and CI have average porosities of 24.7%, 9.5%, and 35.0% (69). Based on the relative fall frequency of these meteorites on Earth (22), the weighted average porosity of these meteorite types is ∼25%. Chondritic IDPs have similar porosities to carbonaceous chondrites (61); therefore, a 25% porosity may also represent well the nucleobase-containing IDPs.

The constrictivity of a porous medium is only important when the size of the species is comparable to the diameter of the pores (68). Therefore, given that nucleobases are <1 nm in diameter and the bulk of pore diameters in, for example, the Acfer 094 carbonaceous chondrite, range from 20 nm to 200 nm (63), we can neglect δ from the listed models.

Tortuosities of chondritic meteorites have an average value of 1.45 (70), and the empirical exponent m for carbonaceous meteorites might be similar to that of nearshore sediments, with a value of 2 (68).

Finally, the free water diffusion coefficient of a single nucleobase has not been measured, however the free water diffusion coefficient of a single nucleotide is 400 $\mu m^2 \cdot s^{-1}$ (71). Since nucleotides are heavier than nucleobases by a ribose and phosphate molecule, they will likely diffuse slower than nucleobases. Therefore, 400 $\mu m^2 \cdot s^{-1}$ is a good estimate of the lower limit of the free water diffusion coefficient of a single nucleobase.

Using the above estimates, we calculate the effective diffusion coefficients for nucleobases in carbonaceous meteorites and IDPs using each of the four models and display them in their respective columns in Table S3. The average value of the effective diffusion coefficient across all four models is 5.36×10^{-11} $m^2 \cdot s^{-1}$.

As previously stated, convective velocity within the pores of carbonaceous IDPs and meteorites is considered negligible. However, this is not the case within 1- to 10-m-radius WLPs. Due to the day–night cycles of Earth, WLPs likely experienced a temperature gradient from the atmospherically exposed top of the pond to the constant geothermally heated base. Since convection is likely the dominant form of heat transport within hydrothermal ponds (72), convection cells would have formed, with warm (higher pressure) parcels of water flowing upward and recently cooled (lower pressure) parcels flowing downward.

The convective fluid velocity can be estimated with the equation

$$u = \sqrt{g\beta\Delta T L} \quad [\mathrm{m \cdot s^{-1}}], \qquad \textbf{[S41]}$$

where g is the gravitational acceleration experienced by the fluid (meters per square second), β is the fluid's volumetric thermal expansion coefficient (per kelvin), and ΔT is the temperature difference (kelvins) over a scale length L (meters) (73). The volumetric thermal expansion coefficients for water at 50 °C, 65 °C, and 80 °C are 4.7, 5.6, and 6.5×10^{-4} K^{-1}, respectively (74).

Small ponds and even lakes can experience a temperature difference of 1 °C to 5 °C over the course of a day–night cycle (75). However, convection begins cycling water well before temperature differences of this magnitude are reached. To estimate the lower bound of a constant temperature difference between the surface and the base of a WLP during a day-to-night period, we assume that each convection cycle cools a surface parcel of water by ΔT. Then, given ΔT, we match the corresponding cycle length and number of cycles with the ∼12-h period required for a 1 °C change in pond temperature. The equation for this calculation is summarized as

$$\Delta T = \left(\frac{2LT_c}{P_{dn}\sqrt{g\beta L}} \right)^{\frac{2}{3}} \quad [\mathrm{K}], \qquad \textbf{[S42]}$$

where T_c is the change in pond temperature over a day-to-night period (kelvins) and P_{dn} is the duration of that period (seconds).

Using Eq. **S42**, the minimum constant temperature difference between the surface and the base of a cylindrical WLP with a radius and depth of 1 m, at 65 °C, is ∼0.007 K. For a WLP with a radius and depth of 10 m, this minimum constant temperature difference increases to ∼0.016 K. However, given that smaller ponds experience greater temperature changes than larger ponds due to faster heat transfer, a ΔT of ∼0.01 K may be a reasonable lower-bound estimate for all WLPs in the 1- to 10-m-radius/depth range.

Given a constant temperature difference of 0.01 K between the base and surface of 1-, 5-, and 10-m-deep WLPs at around 65 °C, the convective flow velocities would be ∼0.7, 1.7, and 2.4 $cm \cdot s^{-1}$, respectively.

Due to the 1D nature of our simulations, we are assuming a radially symmetric outflow of nucleobases from spherical carbonaceous IDPs and meteorites. We also assume that local concentrations of nucleobases that recently flowed out of these sources will remain within a single convection cell. Lastly, we assume that the nucleobase homogenization timescale within a 1D convection cell of a WLP is mostly representative of the nucleobase homogenization timescale within the entire WLP. Although the 1D handling of this part of our model is a simplification of advection and diffusion within WLPs, since we are only attempting to estimate nucleobase homogenization timescales to within a few factors, a 1D model is probably sufficient.

For both model parts, we use a backward time, centered space (BTCS) finite difference method for the diffusion term in the advection–diffusion equation. For part two of the model, we use the upwind method to approximate the additional advection term. The BTCS method was selected over the more accurate Crank–Nicolson method based on the former's stability for sharply edged initial conditions and convergence for increasing levels of refinement. However, differences in diffusion timescales are found to be within rounding error upon comparison of these methods for a 100-μm carbonaceous IDP. The upwind method was selected over higher-order advection approximation methods (e.g., Beam–Warming, Lax–Wendroff) due to its lack of spurious oscillations, lowest error accumulation in mass conservation tests, and convergence for increasing levels of refinement. These two models are summarized in Table S4.

For part one of our nucleobase transport model, the simulation frame starts at the center of the IDP or meteorite, and ends at the rock–pond interface. The left ($r = 0$) boundary is Neumann (i.e., $\partial C_i/\partial t = 0$ across the boundary), simulating zero inflow, and the right boundary is open (i.e., $\partial C_i/\partial t$ before the boundary equals $\partial C_i/\partial t$ after the boundary), simulating outflow into the WLP. The nucleobase contents of the modeled sources are initially homogeneous, but drop sharply to zero at the open boundary (i.e., the initial condition represents an exponentially smoothed step function). This is made to represent the searing of the outermost layer of carbonaceous IDPs and meteorites from atmospheric entry heating.

For part two, the simulation frame is an eccentric 1D convection cell, which loops between the bottom and the top of the WLP (length = $2r_p$). The convection cell is modeled with cyclic boundaries, i.e., continuous nucleobase flow, and no nucleobases

exit the convection cell. The initial concentration of nucleobases is a sharp Gaussian beginning at the base of the pond. The width of the spike is ∼1% of the WLP's radius.

Example simulations, including initial conditions, for parts one and two of our nucleobase transport model are plotted in Fig. S12. Because the time it takes for complete nucleobase outflow from a source, or complete nucleobase homogenization in a WLP, is independent of initial nucleobase abundance, the solution to the diffusion equation at each grid point is displayed as a fraction of the total initial nucleobase concentration. For ease of viewing, part two of the model is displayed in the convection cell's moving frame, with coordinate $r' = r - u\Delta t$.

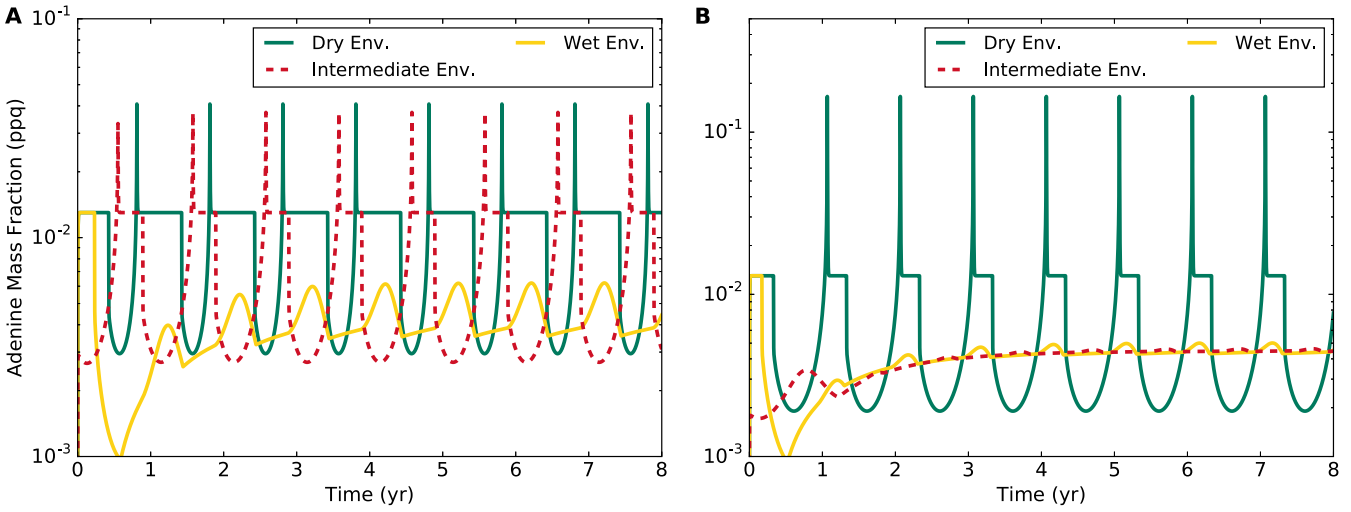

Fig. S1. The accumulation of adenine from only carbonaceous IDP sources in cylindrical WLPs with radii and depths of 1 m. The three curves (dry, intermediate, and wet environments) differ by their precipitation rates, which are from a variety of locations on Earth today, and represent two classes of matching early Earth analogues: hot (Columbia, Indonesia, Cameroon) and warm (Thailand, Brazil, and Mexico) (for details see Table 1). (*A*) The degenerate WLP models used for these calculations correspond to a hot early Earth at 65 °C and a warm early Earth at 20 °C. (*B*) The degenerate WLP models used for these calculations correspond to a hot early Earth at 50 °C and a warm early Earth at 5 °C. Env, environment.

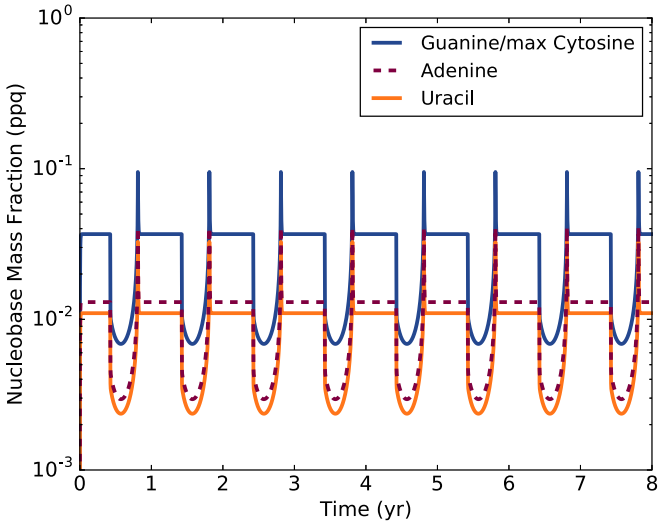

Fig. S2. The accumulation of guanine, adenine, uracil, and cytosine from only carbonaceous IDP sources in cylindrical WLPs with radii and depths of 1 m. The degenerate dry WLP models used for these calculations correspond to a hot early Earth at 65 °C and a warm early Earth at 20 °C. Precipitation rates from Cameroon and Mexico on Earth today are used to represent the hot and warm early Earth analogues, respectively (for details, see Table 1). The cytosine abundance in IDPs used to calculate the maximum cytosine curve matches the average abundance of guanine in IDPs (Table S2). The curves are obtained by numerically solving Eq. **S34**.

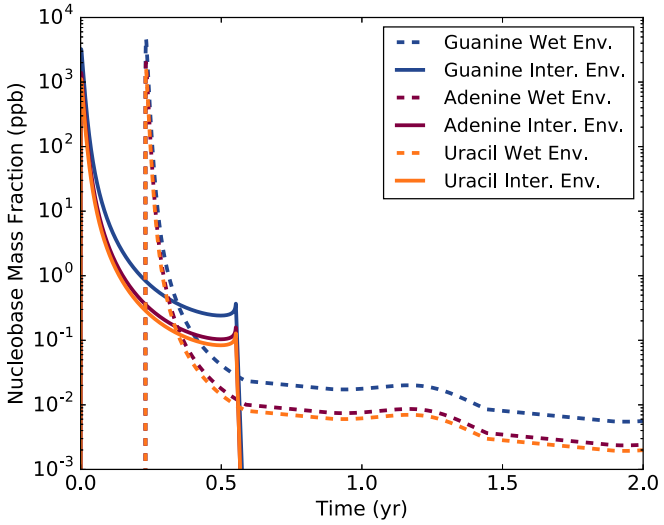

Fig. S3. The accumulation of guanine, adenine, and uracil from 1-cm fragments of an initially 40-m-radius carbonaceous meteoroid in cylindrical WLPs with radii and depths of 1 m. The degenerate WLP models used for these calculations correspond to a hot early Earth at 65 °C and a warm early Earth at 20 °C. The two curves for each nucleobase differ by their precipitation rates, which create intermediate (solid lines) and wet (dotted lines) environments, and are from a variety of locations on Earth today, representing two classes of matching early Earth analogues: hot (Columbia, Indonesia) and warm (Thailand, Brazil) (for details, see Table 1). The curves are obtained by numerically solving Equation **S38**. Env, environment.

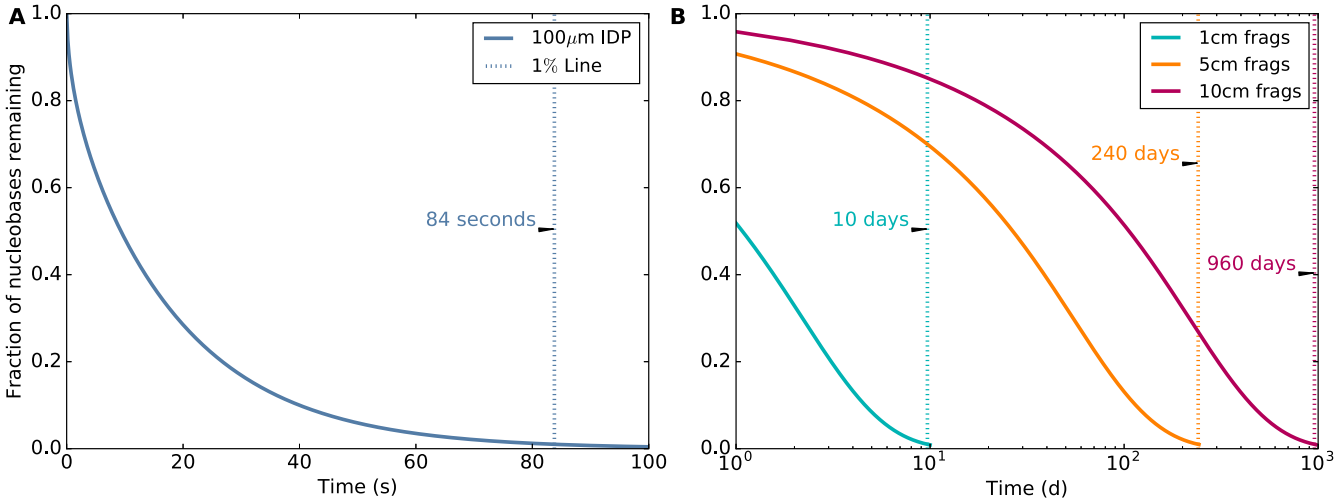

Fig. S4. Fraction of the total initial nucleobases remaining in (*A*) a 100-μm-radius IDP and (*B*) 1-, 5-, and 10-cm-radii meteorites over time as a result of diffusion across a rock–pond boundary. The IDP and meteorites are considered to be lying on the bottom of a WLP, and are diffusing nucleobases symmetrically in the radial direction. The times at which 99% of the initial contained nucleobases have diffused into the WLP are labeled on the plots.

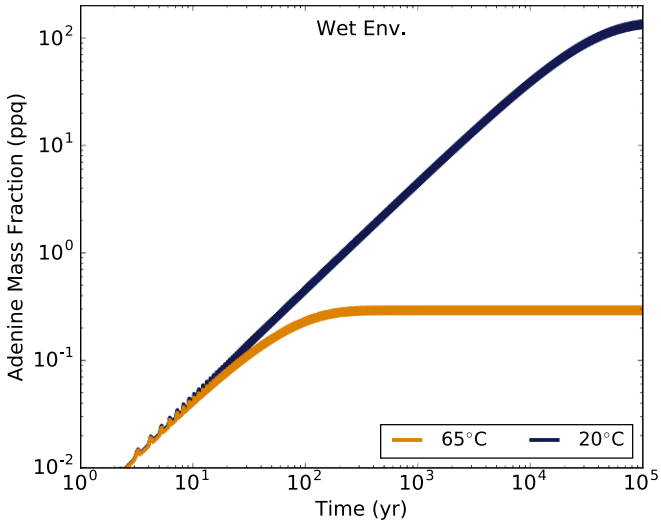

Fig. S5. The no seepage limit: the accumulation of adenine from only carbonaceous IDP sources in cylindrical WLPs with radii and depths of 1 m. The two curves represent the adenine concentrations in a wet environment pond on a hot (65 °C) and warm (20 °C) early Earth (for details, see Table 1). The thickness of the lines is due to the seasonal oscillations in adenine concentrations. Env, environment.

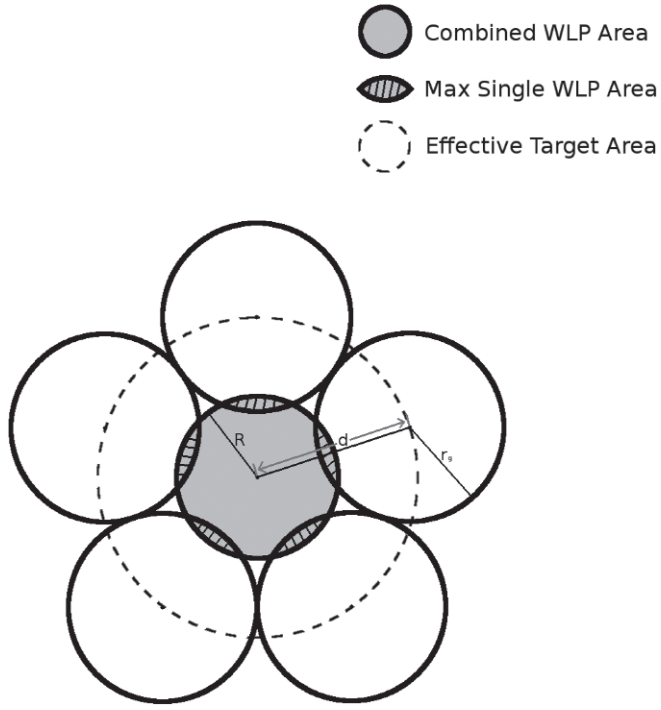

Fig. S6. The dotted circle represents the target area for landing the dispersed fragments from a single meteoroid into any WLP on early Earth. The smaller, light gray circle in the center is the total combined WLP surface area on early Earth at a given time (WLPs would have been individually scattered; however, for a geometric probability calculation, they can be visualized as a single pond cross-section). The larger, surrounding circles represent the area of debris when the fragments of the meteoroid hit the ground. Shortly after 4.5 Ga, the area of debris from a single meteoroid would be large compared with the combined WLP surface area. At any time, the target area for a meteoroid to deposit fragments homogeneously into at least one WLP is slightly larger than the combined area of WLPs. The effective target area grows linearly with total WLP surface area. The diagonally striped intersections between the circles represent the largest individual WLP for which the meteoroid fragment deposition probability is being calculated. The logic is that, if a meteoroid enters the atmosphere at distance *d* from the center of the combined pond cross-section, at least one pond of any size in the WLP distribution will completely overlap with the area of debris.

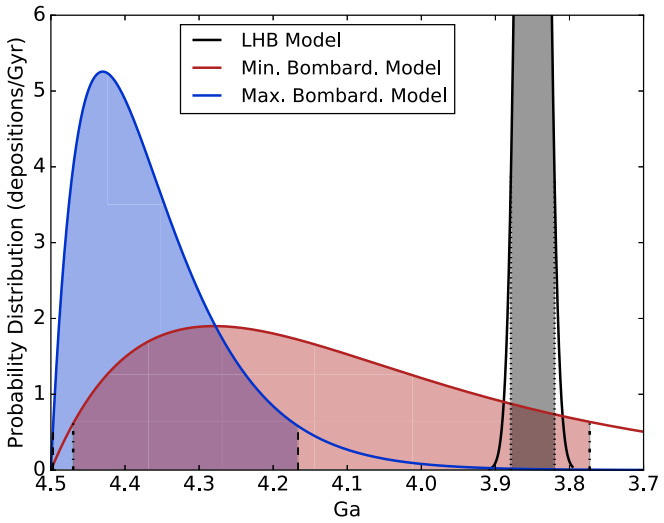

Fig. S7. Normalized probability distributions of fragments from CM-, CI-, and CR-type meteoroids with radii 20 m to 40 m landing in WLPs on early Earth of radii 1 m to 10 m. Three models for mass delivery are compared: the LHB model, and minimum and maximum mass models for a sustained, declining bombardment preceding 3.9 Ga. All models are based on analyses of the lunar cratering record (6, 21). See Fig. 1 for display of mass delivery rates. The 95% confidence intervals are shaded, and correspond to the most likely deposition intervals for each model.

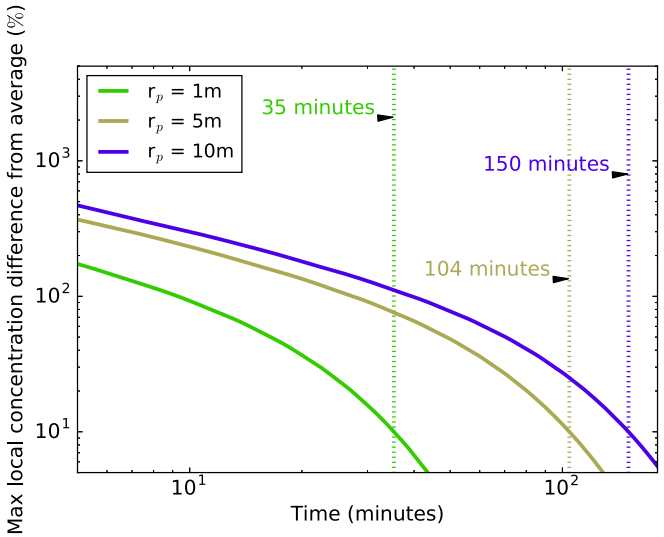

Fig. S8. The nucleobase mixing time in a base-to-surface convection cell (length = $2r_p$) within 1-, 5-, and 10-m-deep WLPs, beginning from a local concentration at the base of the pond. Nucleobase mixing is measured using the maximum percent local nucleobase concentration difference from the average. The time at which the maximum local nucleobase concentration difference from the average drops to 10% is labeled on the plot for each pond size. At this time, we consider the nucleobases in the WLP to be well mixed. For WLPs with radii 1, 5, and 10 m, the convection cell nucleobase mixing times are 35, 104, and 150 min, respectively.

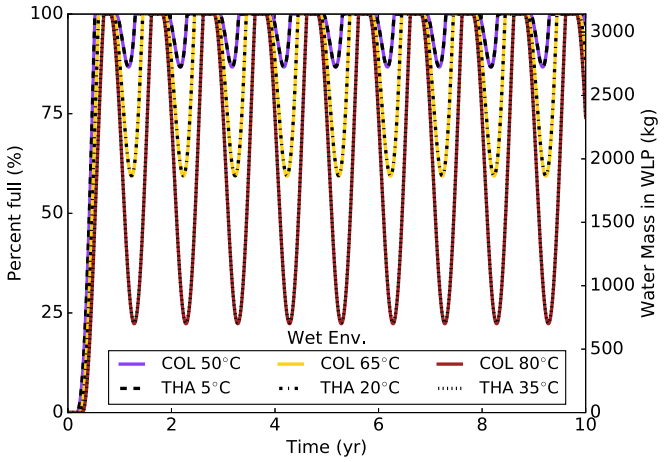

Fig. S9. The effect of temperature on the change in water mass over time in wet environment cylindrical WLPs with radii and depths of 1 m. Temperatures are varied for a hot early Earth model (50 °C, 65 °C, and 80 °C) and a warm early Earth model (5 °C, 20 °C, and 35 °C). Precipitation rates from Columbia and Thailand on Earth today are used to represent the hot and warm early Earth analogues, respectively (for details, see Table 1). COL, Columbia; THA, Thailand.

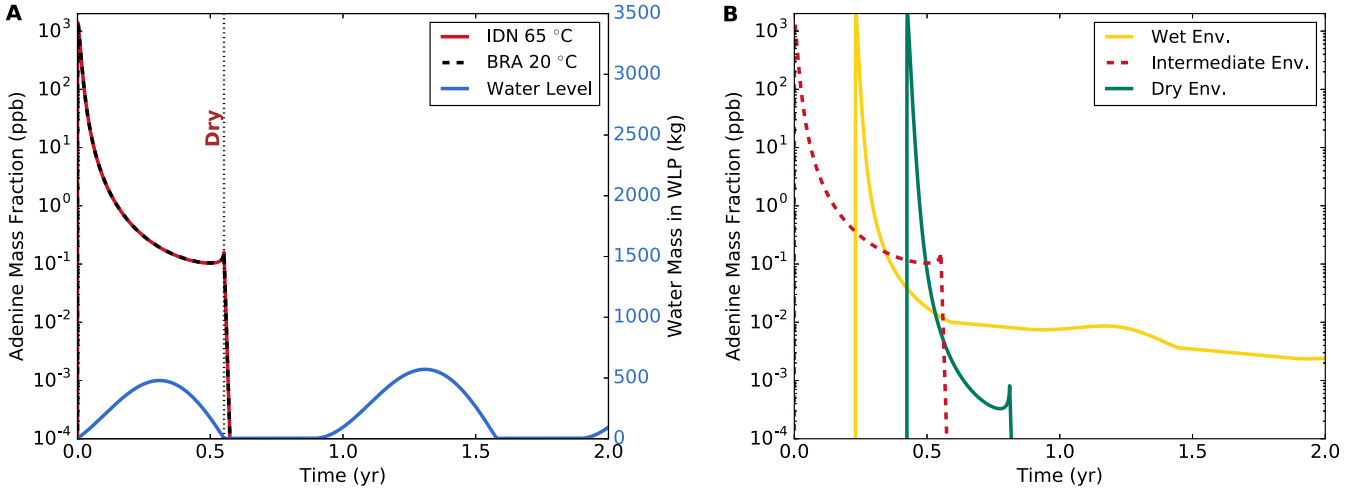

Fig. S10. The accumulation of adenine from 1-cm fragments of an initially 40-m-radius carbonaceous meteoroid in a cylindrical WLP with a radius and depth of 1 m. The degenerate WLP models used for these calculations correspond to a hot early Earth at 65 °C and a warm early Earth at 20 °C. (*A*) The accumulation of adenine from carbonaceous meteorites in an intermediate environment (for details, see Table 1). The wet–dry cycles of the pond are also shown to illustrate the effect of water level on adenine concentration. (*B*) The three curves (dry, intermediate, and wet environments) differ by their precipitation rates, which are from a variety of locations on Earth today, and represent two classes of matching early Earth analogues: hot (Columbia, Indonesia, Cameroon) and warm (Thailand, Brazil, and Mexico) (for details, see Table 1). The curves are obtained by numerically solving Eq. **S38**. BRA, Brazil; Env, environment; IDN, Indonesia.

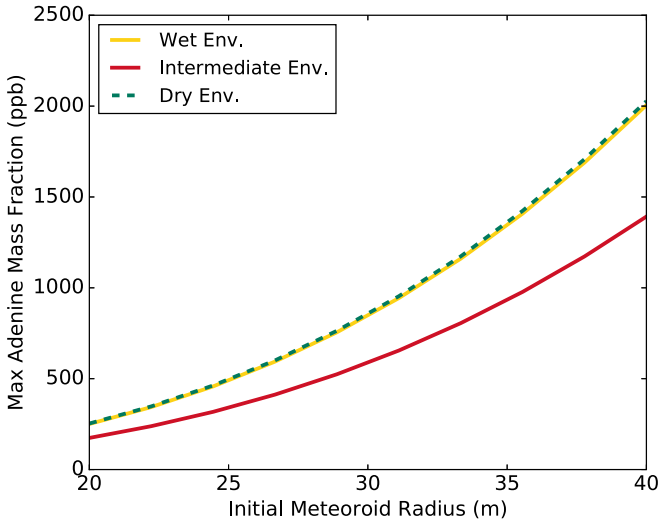

Fig. S11. The maximum concentration of adenine accumulated from 1-cm fragments of a carbonaceous meteoroid 20 m to 40 m in radius in cylindrical WLPs with radii and depths of 1 m. The degenerate WLP models used for these calculations correspond to a hot early Earth at 65 °C and a warm early Earth at 20 °C. The three curves (dry, intermediate, and wet environments) differ by their precipitation rates, which are from a variety of locations on Earth today, and represent two classes of matching early Earth analogues: hot (Columbia, Indonesia, Cameroon) and warm (Thailand, Brazil, and Mexico) (for details, see Table 1). The curves are obtained by numerically solving Eq. **S38**. Env, environment.

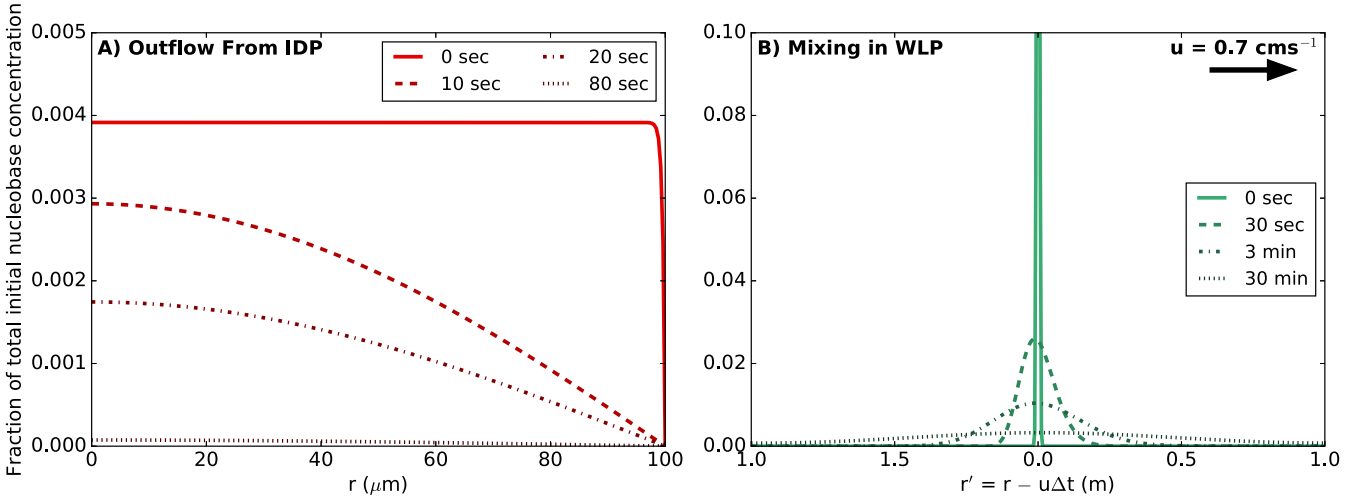

Fig. S12. Example simulations, including the initial conditions, for our two-part nucleobase transport model. Each line represents a different snapshot in time. (*A*) Initially homogeneous nucleobase diffusion from a 100-μm-radius carbonaceous IDP. (*B*) Initially locally concentrated nucleobase mixing in a convection cell within a 1-m-deep WLP. The convection cell is an $L = 2r_p$ eccentric loop flowing between the bottom and the top of the WLP. This loop is sliced at $r' = 1$ m in the convection cell's moving frame and unraveled for display in the 1D plot in *B*.

Table S1. Sources and sinks of pond water and nucleobases in our model of early Earth WLPs

Ingredient	Sources	Sinks
Pond water	Precipitation	Evaporation
		Seepage
Nucleobases	IDPs	Hydrolysis*
	Meteorites*	Seepage*
		Photodissociation†
		Forming nucleotides‡

*Only when pond is wet.
†Only when pond is dry.
‡To be added in a future model.

Table S2. Average guanine, adenine, and uracil abundances (in parts per billion) in the CM, CR, and CI carbonaceous chondrites

Meteorite type	Guanine	Adenine	Uracil
CM	183.5	69.8	50.0
CR	1.8	9.3	—
CI	81.5	60.5	73.0
Weighted average	141.3	60.7	48.6

Abundances obtained from ref. 13. Some CM and CR meteorite analyses found no adenine or uracil; these samples were excluded from the average. Weighted nucleobase averages are also displayed based on relative fall frequencies (22). Uracil has not been measured in CR meteorites. Cytosine has not been measured in any meteorites.

Table S3. Different equations for modeling the effective diffusion coefficient of species in porous media

D_{eff}	Ref.	Estimate for this work, $\times 10^{-11}$ m^2·s^{-1}
$\frac{\phi\delta}{\tau} D_{fw}$	65	6.90
$\frac{\phi\delta}{\tau^2} D_{fw}$	66	4.76
$\frac{2\phi}{3-\phi} D_{fw}$	67	7.27
$\phi^m D_{fw}$	68	2.50

Estimates of the effective diffusion coefficients of single nucleobases through the pores of carbonaceous IDPs and meteorites are also calculated for each model. The free water diffusion coefficient, D_0, represents the unobstructed diffusion of a species; the porosity factor, ϕ, represents the void fraction of the medium; the constrictivity factor, δ, represents the bottleneck effect due to small pore diameters; and the tortuosity factor, τ, represents the restriction in diffusive flow due to curves in the pores. Estimates of these factors, and the empirical exponent, m, for carbonaceous IDPs and meteorites are $D_0 = 4 \times 10^{-10}$ m^2·s^{-1}, $\phi = 0.25$, $\delta = 1$, $\tau = 1.45$, and $m = 2$ (68–71). D_{fw}, free water diffusion coefficient; ϕ, porosity; δ, constrictivity; τ, tortuosity; m, empirical exponent.

Table S4. Summary of parts one and two of our 1D nucleobase transport model

Part	Model description	Numerical method	Boundaries	Initial condition	ϕ	D_{eff}, m^2·s^{-1}
1	Nucleobase outflow from carbonaceous IDPs and meteorites	BTCS	Neumann and open	See Fig. S12*A*	0.25	5.36×10^{-11}
2	Nucleobase mixing in WLPs	BTCS and upwind	Cyclic	See Fig. S12*B*	1	4.0×10^{-10}

Part one is a model of nucleobase outflow from carbonaceous IDPs and meteorites while they lie at the base of a WLP. Part two is the mixing (i.e., homogenization) of a local concentration of nucleobases throughout the WLP.